


A single-cell massively parallel reporter assay detects cell-type-specific gene regulation

Received: 7 December 2021

Accepted: 5 December 2022

Published online: 12 January 2023

 Check for updates


Siqi Zhao^{1,2,4}, Clarice K. Y. Hong^{1,2}, Connie A. Myers³, David M. Granas^{1,2}, Michael A. White^{1,2}, Joseph C. Corbo³ & Barak A. Cohen^{1,2} 

Massively parallel reporter gene assays are key tools in regulatory genomics but cannot be used to identify cell-type-specific regulatory elements without performing assays serially across different cell types. To address this problem, we developed a single-cell massively parallel reporter assay (scMPRA) to measure the activity of libraries of *cis*-regulatory sequences (CRSs) across multiple cell types simultaneously. We assayed a library of core promoters in a mixture of HEK293 and K562 cells and showed that scMPRA is a reproducible, highly parallel, single-cell reporter gene assay that detects cell-type-specific *cis*-regulatory activity. We then measured a library of promoter variants across multiple cell types in live mouse retinas and showed that subtle genetic variants can produce cell-type-specific effects on *cis*-regulatory activity. We anticipate that scMPRA will be widely applicable for studying the role of CRSs across diverse cell types.

The majority of heritable variation for human diseases maps to the noncoding portions of the genome^{1–6}. This observation has led to the hypothesis that genetic variation in the *cis*-regulatory sequences (CRSs) that control gene expression underlies a large fraction of disease burden^{7–10}. Because many CRSs function only in specific cell types¹¹, there is intense interest in high-throughput assays that can measure the effects of cell-type-specific CRSs and their genetic variants.

Massively parallel reporter assays (MPRAs) are one family of techniques that allow investigators to assay libraries of CRSs and their noncoding variants en masse^{12–18}. In an MPRA experiment, every CRS drives a reporter gene carrying a unique DNA barcode in its 3' UTR, which allows investigators to quantify the activity of each CRS by the ratio of its barcode abundances in the output RNA and input DNA. This approach allows investigators to identify new CRSs, assay the effects of noncoding variants and discover general rules governing the functions of CRSs^{12,19–23}. One limitation of MPRAs is that they are generally performed in monocultures or as bulk assays across the cell types of tissues. Performing cell-type-specific MPRAs in tissues will require methods to simultaneously read out reporter gene activities and cell-type information in heterogeneous pools of cells.

To address this problem, we developed single-cell MPRA (scMPRA), a procedure that combines single-cell RNA sequencing with MPRA. scMPRA simultaneously measures the activities of reporter genes in single cells and the identities of those cells using their single-cell transcriptomes. The key component of scMPRA is a two-level barcoding scheme that allows us to measure the copy number of all reporter genes present in a single cell from mRNA alone. A specific barcode marks each CRS of interest (CRS barcode, 'cBC'), and a second random barcode (rBC) acts as a proxy for the DNA copy number of reporter genes in single cells (Fig. 1a). The critical aspect of the rBC is that it is complex enough to ensure that the probability of the same cBC and rBC appearing in the same cell more than once is vanishingly small. In this regime, the number of different cBC–rBC pairs in a single cell becomes an effective proxy for the copy number of a CRS in that cell. Even if a cell carries reporter genes for multiple different CRSs and each of those reporter genes is at a different copy number, we can still normalize each reporter gene in each individual cell to its plasmid copy number. With this barcoding scheme, we can measure the activity of many CRSs with different input abundances at single-cell resolution, which allows us to measure the activity of CRSs simultaneously across different populations of cells.

¹Edison Family Center for Systems Biology and Genome Sciences, Washington University School of Medicine, St. Louis, MO, USA. ²Department of Genetics, Washington University School of Medicine, St. Louis, MO, USA. ³Department of Pathology and Immunology, Washington University School of Medicine, St. Louis, MO, USA. ⁴Present address: Ginkgo Bioworks, Boston, MA, USA.  e-mail: cohen@wustl.edu

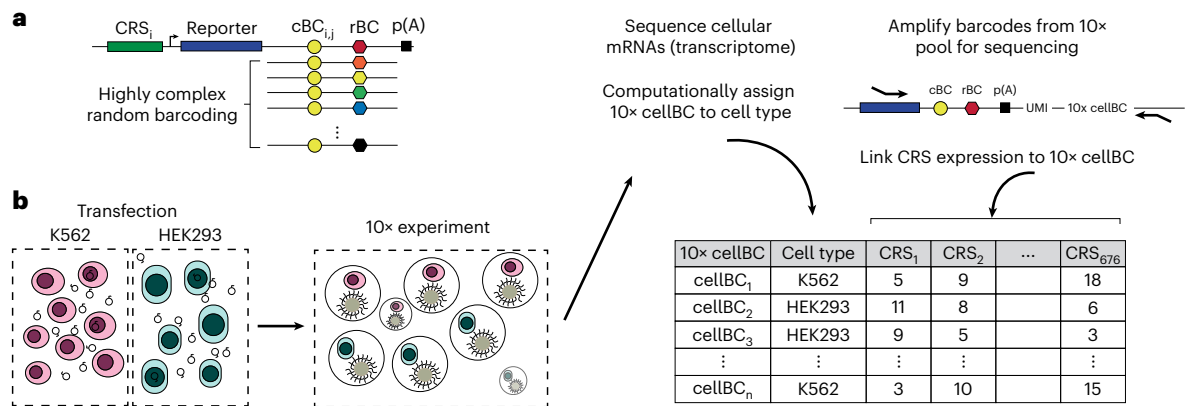


Fig. 1 | scMPRA measures CRS activity at single-cell resolution. a, Each CRS reporter construct is barcoded with a cBC that specifies the identity of the CRS, and a highly complex rBC. The complexity of the cBC–rBC pair ensures that the probability of identical plasmids being introduced into the same cell is extremely low. **b**, Experimental overview for scMPRA using the mixed-cell experiment as an example. K562 cells and HEK293 cells are transfected with the double-barcoded

core promoter library. After 24 h, cells were collected and mixed for 10x scRNA-seq. Cell identities were obtained by sequencing the transcriptome, and single-cell expression from CRSs was obtained by quantifying the barcodes. The cell identity and CRS activities (as measured by the cBC–rBC abundances) were linked by the shared 10x cell barcodes.

Results

scMPRA enables single-cell measurement of CRS activity

As a proof of principle, we first used scMPRA to test whether different classes of core promoters show different activities in different cell types. Core promoters are the noncoding sequences that surround transcription start sites, where general cofactors interact with RNA polymerase II^{24,25}. Core promoters are divided into different classes by the functions of their host genes (housekeeping versus developmental) and by the sequence motifs they contain (TATA box, downstream promoter element (DPE), and CpG islands)²⁶. We selected 676 core promoters that we previously tested^{24,25} and cloned them into a double-barcoded MPRA library. Given the complexity of the library (>1 × 10⁷ unique cBC–rBC pairs), we calculated that the probability of plasmids with the same cBC–rBC pair occurring in the same cell is less than 0.01 with our transfection protocols (Methods). Given this low likelihood, the number of rBCs per cBC in a cell represents the copy number of a CRS in that cell. Knowing the copy number of CRSs in single cells allows us to normalize reporter gene expression from each CRS to its copy number in individual cells.

We performed a cell mixing experiment to test whether scMPRA could measure cell-type-specific expression of reporter genes. We transfected K562 (chronic myelogenous leukemia) and HEK293 (human embryonic kidney) cells and performed scMPRA on a 1:1 mixture of those cell lines (Fig. 1b). The mRNA from single cells was captured, converted to cDNA and sequenced. The resulting cBC–rBC abundances and transcriptome of each single cell are linked by their shared 10x cell barcode.

We recovered a total of 3,112 cells (97%) that could be unambiguously assigned to one of the two cell types (Fig. 2a and Extended Data Fig. 1a,b) and computed the mean expression of each core promoter in the library in each cell type (Methods). The measurements were reproducible in both cell types (K562–Pearson’s $R = 0.89$, Spearman’s $\rho = 0.57$; HEK293–Pearson’s $R = 0.96$, Spearman’s $\rho = 0.92$; Fig. 2b,c and Supplementary Table 1), and we obtained measurements for 99.5% of core promoters in K562 cells and 100% in HEK293 cells, highlighting the efficiency of scMPRA. The median number of cells in which each core promoter was measured was 76 for K562 cells and 287 for HEK293 cells (Fig. 2d,e). We also tabulated the number of cBC–rBC pairs in each individual cell and found that the median per cell was 164 in K562 cells and 341 in HEK293 cells (Extended Data Fig. 1c,d). On average we detected ten rBCs per promoter in individual HEK293 cells and two rBCs per promoter in K562 cells (Extended Data Fig. 1e,f). To validate

the scMPRA measurements, we conducted bulk MPRA of the core promoter library in the two cell types separately. Bulk MPRA measurements are not corrected for PCR amplification biases with Unique Molecular Identifiers (UMIs), and we found that the bulk measurements correlate well with aggregated single-cell measurements without UMI correction (Fig. 2f,g). That correlation drops with the UMI-corrected single-cell measurements (Extended Data Fig. 1g,h), which suggests that bulk measurements may suffer from overcounting because of uneven amplification during PCR.

scMPRA detects cell-type-specific CRS activity

We asked whether the data allowed us to detect core promoters with differential activity between K562 and HEK293 cells. While different classes of core promoters generally had similar activities in both cell lines (Fig. 2h), our differential analysis using DESeq2 (ref. 27) identified a small number of promoters (11 of 669) that are upregulated in K562 cells and 59 promoters that are downregulated in K562 cells (adjusted $P < 0.01$, log₂ fold change > 0.3; Fig. 2i and Supplementary Table 2). Among the down-regulated promoters, 48 of 59 core promoters belong to housekeeping genes ($P = 1.08 \times 10^{-11}$; Fig. 2j) and 46 of 59 core promoters are CpG-island-containing core promoters ($P = 2.18 \times 10^{-6}$; Fig. 2k). This result is not due to differences in the quality of measurements between housekeeping and developmental promoters (Extended Data Fig. 1i,j). These results demonstrate the ability of scMPRA to detect CRSs with cell-type-specific activities.

scMPRA detects cell substate-specific CRS activity

Single-cell studies have revealed heterogeneity in cell states even within isogenic cell types^{28–31}. Therefore, we asked if scMPRA can identify CRSs with cell-state-specific activity. We repeated scMPRA on K562 cells alone and obtained a total of 4,041 cells from two biological replicates. Measurements of each library member were again highly correlated between replicates and agree well with independent bulk measurement (Extended Data Fig. 2a,b).

Because the phases of the cell cycle represent distinct cell states, we asked whether scMPRA could identify reporter genes with differential activity through the cell cycle. We assigned cell cycle phases to each cell using their single-cell transcriptome data (Fig. 3a) and calculated the mean expression of each reporter gene in different cell cycle phases. We found that most core promoters in our library are upregulated in the G1 phase of the cell cycle and that some housekeeping promoters are highly expressed through all cell cycle phases

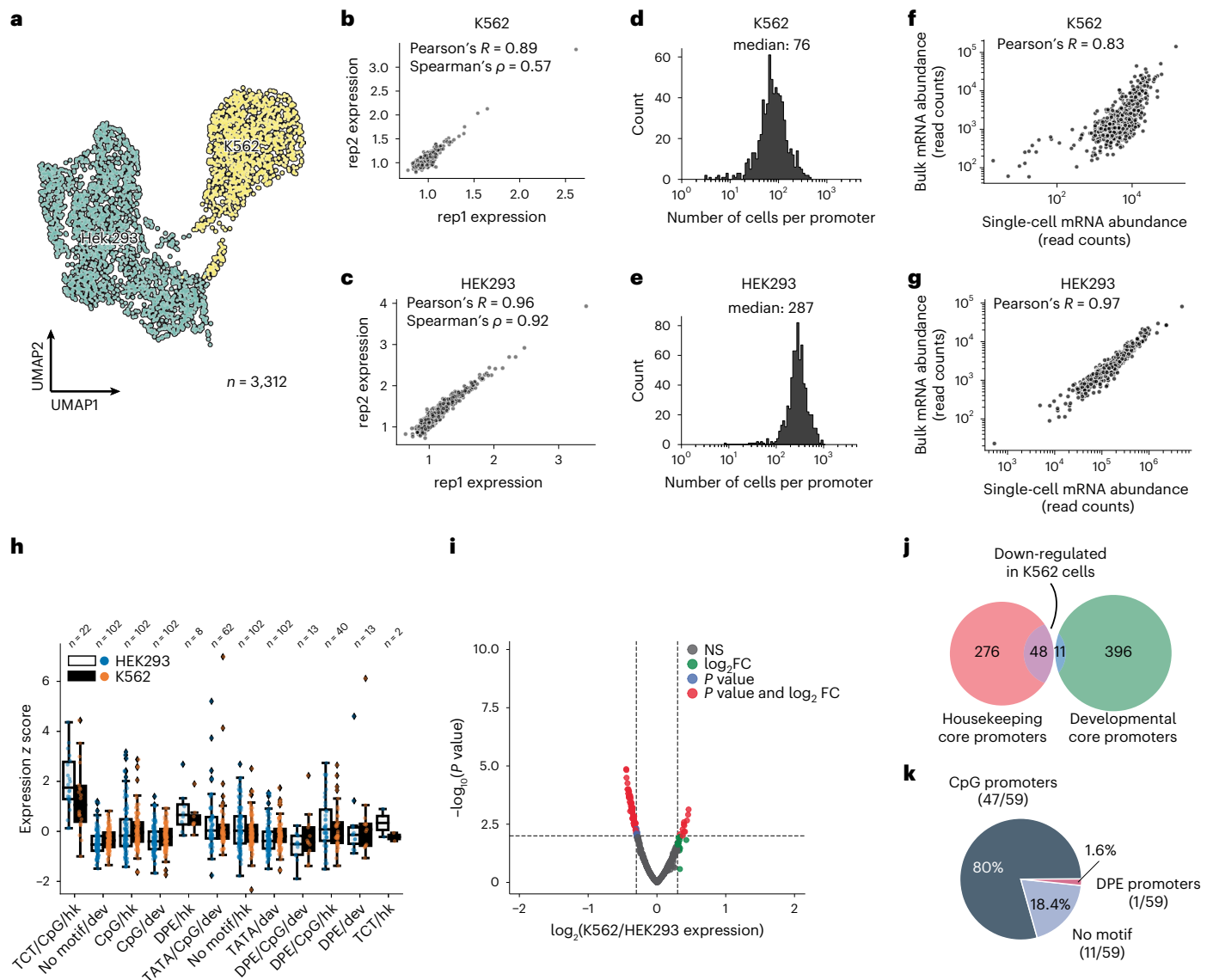


Fig. 2 | scMPRA detects cell-type-specific CRS activity. **a**, UMAP of the transcriptome from the mixed-cell scMPRA experiment. 3,312 of 3,417 cells are assigned to either K562 or HEK293 cells and visualized here. **b,c**, Reproducibility of replicate measurements (rep1 and rep2) of the mean expression from each core promoter in both K562 (**b**) and HEK293 (**c**) cells. **d,e**, Histogram of the number of cells in which each core promoter was measured for HEK293 (**d**) and K562 (**e**) cells. **f,g**, Correlations between scMPRA and bulk MPRA using mRNA abundances (cBC counts per cell) to make the two methods comparable. **h**, Boxplot of the activities of core promoters from different categories in K562 (**f**, orange) and HEK293 (**g**, blue) cells. The promoter categories are taken from ref. 25. Because the average

expression of all promoters was different between K562 and HEK293, we plotted each category according to its deviation from the average expression (z score) of all promoters in each cell type. **i**, Volcano plot for DE of core promoters in K562 and HEK293 cells. Red dots represent substantially DE reporters (two-sided Wald test adjusted $P < 0.01$ and \log_2 fold change > 0.3). **j**, Venn diagram of the functional characterization (housekeeping versus developmental) of down-regulated core promoters in K562 cells. Housekeeping promoters are enriched ($P = 1.08 \times 10^{-11}$ from two-sided hypergeometric test). **k**, Pie chart of the sequence features (CpG, DPE, TATA) of down-regulated core promoters. CpG promoters are enriched ($P = 2.18 \times 10^{-6}$, two-sided hypergeometric test).

(Fig. 3b and Supplementary Table 3). We also identified core promoters with different expression dynamics through the cell cycle. For example, we found that the core promoter of UBA52 remains highly expressed in the S phase, whereas the core promoter of CXCL10 is lowly expressed throughout (Extended Data Fig. 2c). This analysis illustrates the ability of scMPRA to identify CRSs whose activity naturally fluctuates with cellular dynamics.

We then asked whether scMPRA could detect reporter genes with activities that were specific to other cell states in K562 cells, after normalizing for cell cycle effects. We focused on two specific substates that have been reported and experimentally validated for high proliferation rates in K562 cells^{32,33}. The first is the CD34+/CD38⁻ substate

that has been identified as a leukemia stem cell subpopulation and the second is the CD24⁺ substate that is linked to the selective activation of proliferation genes by bromodomain transcription factors^{29,30}. To identify these substates in our single-cell transcriptome data, we first regressed out the cell cycle effects and confirmed that the single-cell transcriptome data no longer clustered by the cell cycle phase (Extended Data Fig. 2d). We then identified clusters within K562 cells that have the CD34+/CD38⁻ expression signature or the CD24⁺ signature (Fig. 3c). Although the CD34+/CD38⁻ cells represent only 9.3% of the cells, scMPRA revealed two distinct classes of core promoters that are upregulated and downregulated in these cells relative to the CD24⁺ and 'differentiated' clusters (Fig. 3d). Conversely, the expression

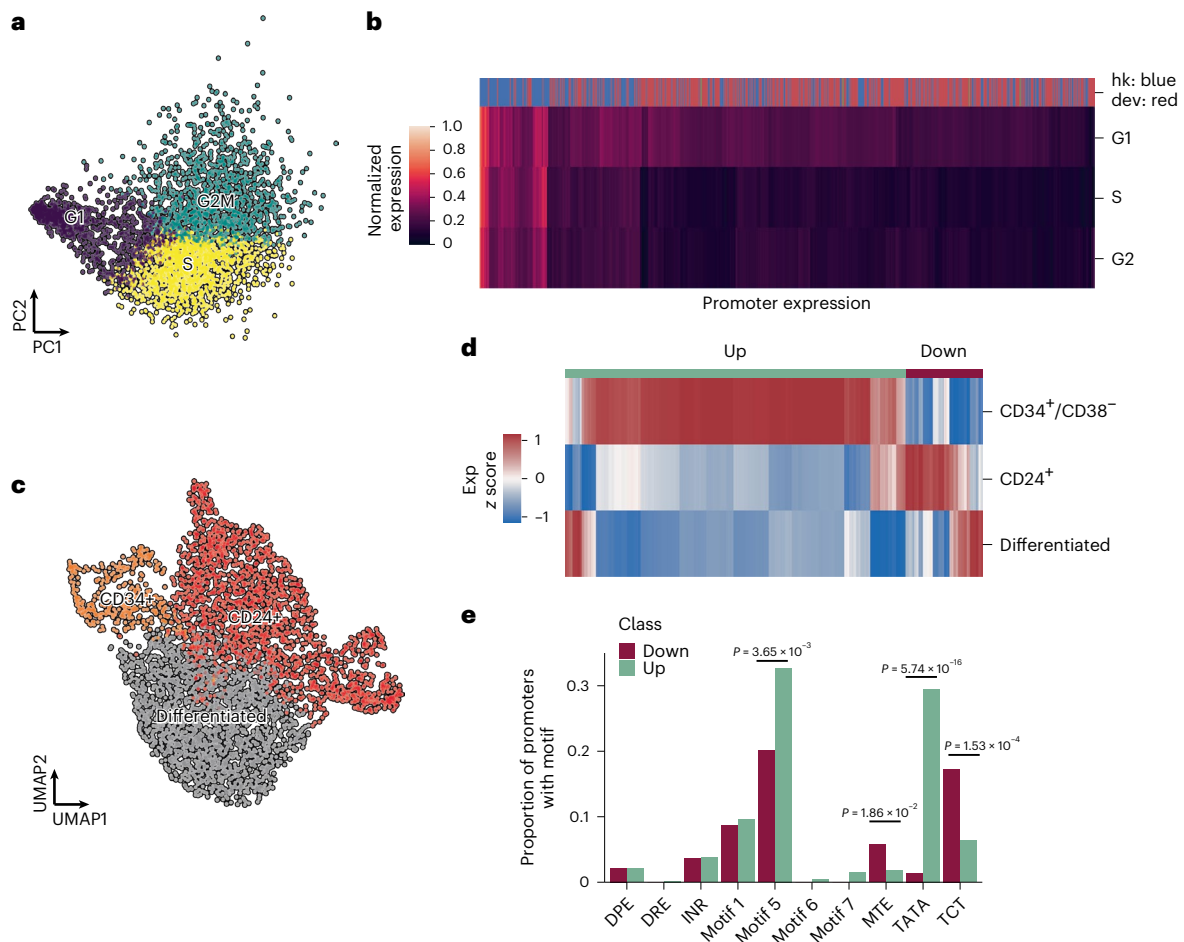


Fig. 3 | scMPRA detects substate-specific CRS activity. **a**, PCA plot of K562 cells ($n = 4,041$) classified by their cell cycle scores. **b**, Heatmap of core promoter activities in different cell cycle phases (color bar indicates housekeeping (blue) versus developmental (red) promoters). Core promoter activities have been normalized within each cell cycle phase to highlight the differences between housekeeping and developmental promoters. **c**, UMAP embedding of K562 cells with high proliferation ($CD34^+/CD38^-$ and $CD24^+$) and undifferentiated substates.

d, Hierarchical clustering showing two clusters ('up' and 'down') based on the expression patterns in the three substates. The promoter ($n = 672$) activities are plotted as their z score from the average across cell states to highlight the difference between cell states. **e**, Proportion of promoters in the up and down clusters that contain the indicated core promoter motif. Significant P values from a two-sided Fisher's exact test are shown.

patterns of promoters are similar between the $CD24^+$ and 'differentiated' clusters (Fig. 3d and Supplementary Table 4). Motif analysis of the upregulated/downregulated classes of promoters in $CD34^+/CD38^-$ cells showed that different core promoter motifs are enriched in each class, with the TATA box and Motif 5 being enriched in the upregulated class and MTE and TCT motifs being enriched in downregulated class (Fig. 3e). This result suggests that differences in core promoter usage might be driving the differences between $CD34^+/CD38^-$ and the other clusters. Because the TATA box is mostly found in developmental core promoters, the $CD34^+/CD38^-$ subpopulation likely reflects the more 'stem-like' cellular environment in these cells. Our analysis highlights the ability of scMPRA to identify CRSs with differential activity in rare cell populations.

scMPRA is reproducible and accurate in mouse retinas

To demonstrate that scMPRA is applicable in a complex tissue with multiple cell types, we performed experiments in explanted mouse retinas. Intact retina from newborn mice can be cultured and transfected ex vivo. This system has been useful for bulk MPRA experiments^{13,19,34}, but the results from those experiments report the aggregate expression of library members across the cell types of the retina. Performing scMPRA in ex vivo retina provided a chance to assay an MPRA library in

a living tissue with multiple cell types in their proper three-dimensional organization.

For this analysis, we designed a library consisting of two independently synthesized wild-type (WT) copies, and 113 variants, of the full-length *Gnb3* promoter (115 library members; Supplementary Table 5). We chose the *Gnb3* promoter because it has high activity in photoreceptors and bipolar cells but lower expression in other interneurons (that is, amacrine cells) and Müller glia cells. The library contains mutations in the known transcription factor binding sites (TFBSs) in the *Gnb3* promoter and mutations that scan across two phylogenetically conserved regions of the promoter (details in Fig. 6 below). We constructed this library of *Gnb3* promoter variants using the double barcoding strategy described above, with one key modification that we now describe.

In the *Gnb3* promoter library, we addressed the inability of scMPRA to measure silent library members. In the first iteration of scMPRA, when a library member produces no mRNA barcodes its corresponding plasmid cannot be detected, and thus, a cell containing a silent plasmid is indistinguishable from a cell without a plasmid. To avoid this potential problem in our retina experiments, we included an additional cassette on the *Gnb3* promoter library that allows us to detect the presence of plasmids carrying silent promoter variants.

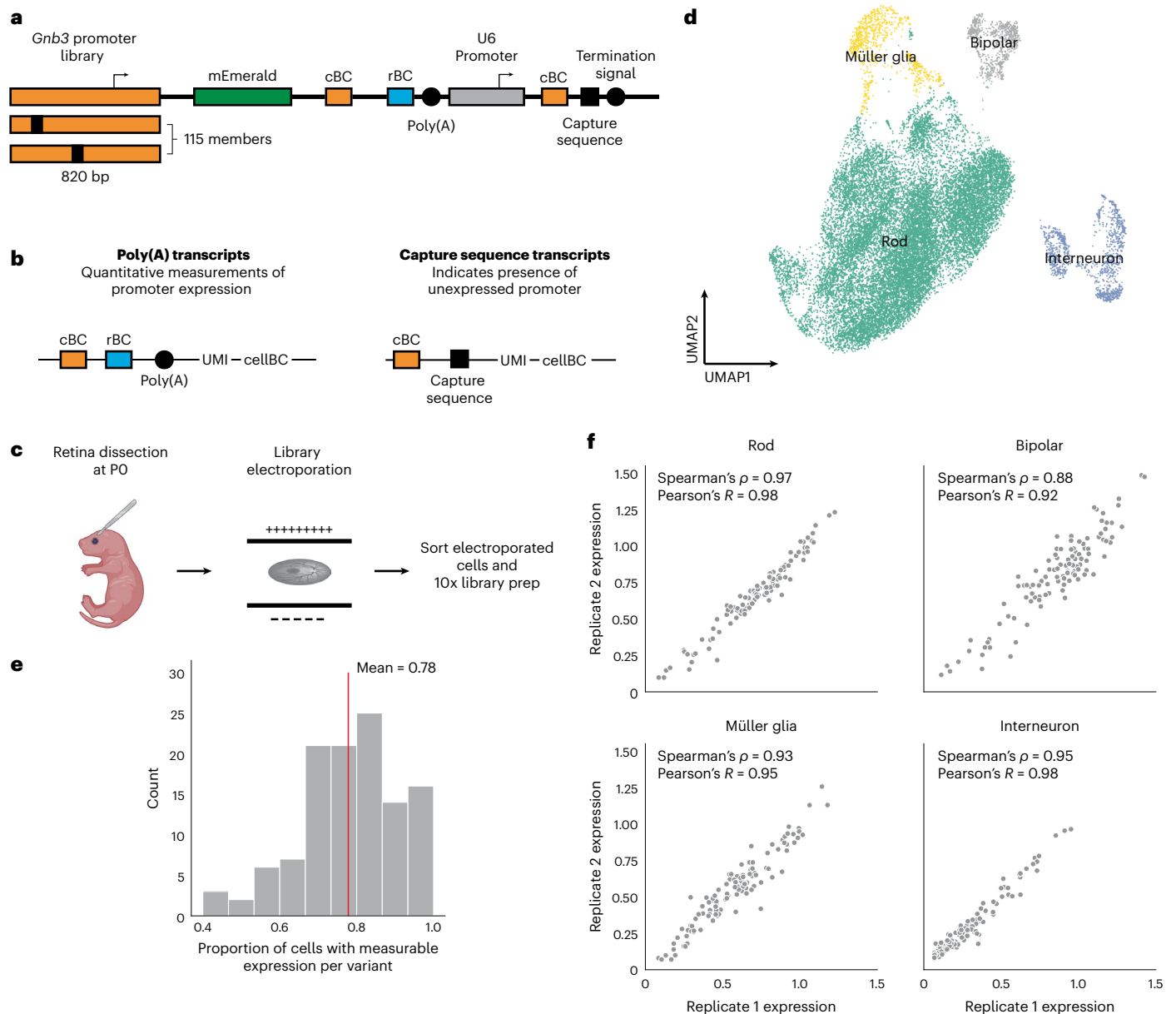


Fig. 4 | scMPRA design and workflow in mouse retina. a, Schematic of *Gnb3* promoter library constructs. In addition to the cBC and rBC barcodes, the *Gnb3* promoter library contains an additional cassette in which the constitutive U6 promoter expresses a second copy of the cBC with a capture sequence for isolating these transcripts on 10x gel beads. **b**, Two different types of transcripts produced from the *Gnb3* promoter library to measure promoter expression and detect unexpressed promoters. The two types of transcripts originating from the

same cell share the same 10x cell barcodes. **c**, Experimental workflow for scMPRA in ex vivo mouse retinas. **d**, UMAP of all cells ($n = 22,161$) measured in scMPRA with four major cell types identified. **e**, For each *Gnb3* variant in the library, we determined the proportion of cells that contain barcoded poly(A) transcripts out of all the cells that contained the variant. **f**, Reproducibility of promoter activities between biological replicates in each of the four major cell types (all 115 promoters were detected in every cell type).

We included a cassette in which the U6 promoter drives the expression of a second copy of the cBC coupled to the 10x Capture Sequence (Fig. 4a). The U6 promoter drives strong RNA Polymerase III-dependent transcription and is independent of the activity of the *Gnb3* promoter. While we do not expect interference between the pol III-dependent U6 promoter and the pol II-dependent *Gnb3* promoter variants, we minimized this possibility by putting the U6 cassette downstream of the *Gnb3* variants and placing a polyA signal between the cassettes. The Capture Sequence is a specific sequence that is typically used to identify gRNAs in Perturb-seq experiments³⁵, but we use it here to isolate U6-expressed cBCs (Fig. 4b). When a cell contains a U6 cBC without the corresponding *Gnb3* promoter cBC, it indicates the presence of a silent library member.

We introduced the *Gnb3* promoter variant library into newborn mouse retinas and assessed the cell types into which the library entered by single-cell RNA sequencing (scRNA-seq; Fig. 4c). We obtained a total of 22,161 cells from two replicate experiments with a mean of 22,528 reads per cell and 1,642 genes identified per cell. The scRNA-seq data showed that we recovered rod photoreceptors (87.3%), bipolar cells (3.5%), interneurons (that is, amacrine cells; 3.9%) and Müller glia cells (5.2%; Fig. 4d and Extended Data Fig. 3a,b).

We then computed the expression of each *Gnb3* promoter variant in each cell type by sequencing the *Gnb3*-expressed barcodes and the U6 barcodes from single cells. Cells with U6-expressed cBC counts, but no *Gnb3*-expressed cBC counts, represented cells in which that promoter variant was silent. On average, *Gnb3* promoter variants were

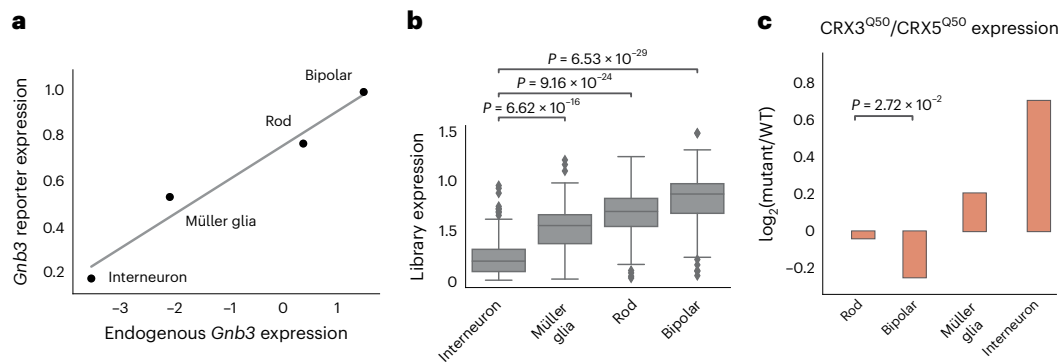


Fig. 5 | scMPRA recapitulates *Gnb3* expression patterns. a, The expression of the wild-type *Gnb3* promoter in scMPRA reflects endogenous expression levels of *Gnb3* in the respective cell types. The solid line represents the best fit linear regression. **b**, The expression of the entire *Gnb3* library ($n = 115$ variants) in different cell types also follows endogenous *Gnb3* expression (P -value from

the two-sided Mann–Whitney U test). **c**, scMPRA recapitulates the effects of a known *Gnb3* variant, where the CRX3^{Q50}/CRX5^{Q50} variant reduces expression in bipolar cells specifically ($*P < 0.05$, P -value from the two-sided Welch’s t test). All expression values are plotted as the mean of two biological replicates.

silent in 22% of cells, but this number varied widely (Fig. 4e) and was linearly related to the strength of the promoter, with stronger promoters expressing in a larger fraction of cells (Extended Data Fig. 3c). Using both the *Gnb3*-driven and U6-driven counts allowed us to compute the average expression of a promoter variant across all the cells of a given cell type, while still accounting for cells in which that promoter variant is silent (Methods).

Biological replicates measurements of the *Gnb3* promoter variant library were reproducible in all four cell types (Fig. 4f and Supplementary Table 6). Reproducibility was highest in rod cells (Spearman’s $\rho = 0.97$, Pearson’s $R = 0.98$) because rod cells are the most abundant cell type in the mouse retina. The reproducibility was slightly lower in the rarer cell types (bipolar cells—Spearman’s $\rho = 0.88$, Pearson’s $R = 0.92$; Müller glia—Spearman’s $\rho = 0.93$, Pearson’s $R = 0.95$ and interneurons—Spearman’s $\rho = 0.95$, Pearson’s $R = 0.98$), but remained high enough to assess the expression of individual library members. We determined how reproducibility scales with the number of cells in scMPRA by subsampling the expression data. The minimum number of cells required for reproducible measurements (Spearman’s $\rho > 0.75$) of mean reporter gene levels is 75 cells (Extended Data Fig. 3d). Our results show that scMPRA works well for measuring reporter gene levels across cell types in complex tissues using small numbers of cells.

Two additional observations suggest that scMPRA measurements are accurate in ex vivo retinas. First, the expression of the wild-type *Gnb3* reporter and the average expression of all *Gnb3* promoter variants correlate with endogenous *Gnb3* expression in the corresponding scRNA-seq data (Fig. 5a,b). Second, our scMPRA data reproduced the known effect of a cell-type-specific *Gnb3* promoter variant. Murphy et al.³⁶ showed that altering two of the K50 homeobox sites in the *Gnb3* promoter to Q50 sites reduces expression in bipolar cells while leaving expression in rod cells relatively unaffected. We observed the same reduction in bipolar cells when compared with rod cells for this same mutation (Fig. 5c). In addition, scMPRA also revealed that this mutation shows increased activity in Müller glia and interneurons. Taken together, these observations demonstrate that scMPRA is reproducible and accurate when applied to cell types in a complex tissue.

scMPRA reveals cell-type-specific promoter variants

The *Gnb3* library was designed to probe components of the promoter including five binding sites for K50-type homeodomain TFs, an E-box binding site and two evolutionarily conserved regions (Fig. 6a). In this experiment, we define the effect of a mutation as its relative fold-change to the WT *Gnb3* promoter in each cell type because the *Gnb3* promoter is expressed at different levels across cell types (Fig. 5a). We labeled the homeobox sites as Cone Rod Homeobox (CRX) sites because CRX is a

K50-homeodomain protein that have an important role in rods and bipolar cells and is required for *Gnb3* expression³⁶. K50-homeodomains contain lysine at the 50th amino acid residue and have different binding preferences from Q50-homeodomains, which contain glutamine at position 50 and are also expressed in the retina.

Inactivating mutations in any individual CRX site decreased *Gnb3* reporter expression in bipolar and rod cells, but deletion of either CRX1 or CRX5 also resulted in increased expression in interneurons (Fig. 6b). The CRX2 disruption had the largest effect on expression, and mutating the CRX2 site in combination with any other CRX site also caused large reductions in expression in rods and bipolar cells. Murphy et al.³⁶ previously reported that different retinal cell types differ in their usage of K50 versus Q50 motifs, suggesting that promoters containing K50 or Q50 motifs may display cell-type-specific differences. Single and double swaps of K50 CRX-binding sites with Q50 binding sites tended to yield cell-type-specific effects, primarily because interneurons displayed larger responses to the Q50 swaps compared with rod and bipolar cells (Fig. 6c). Increasing the affinity of CRX sites tended to have mild effects on expression in rods and bipolar cells but increased expression substantially in interneurons (Fig. 6d). The results from modifying CRX sites demonstrated that perturbations to single-binding sites can produce cell-type-specific effects.

We next examined the effects of single nucleotide changes in the E-box binding site (Fig. 6e). Helix-Loop-Helix transcription factors, which bind E-box motifs, are critical for the development of multiple retinal cell types³⁷. Several single-nucleotide substitutions in the E-box resulted in strong effects on expression, although only one substitution produced significant cell-type-specific effects. While the E-box is critical for strong expression of the *Gnb3* promoter, subtle changes to its sequence do not generally result in cell-type-specific changes to its activity.

To examine the effects of more severe sequence changes and to assess the effects of perturbations outside the known TFBSs, we tiled mutations through the two evolutionarily conserved regions shuffling 5 bp at a time (Fig. 6f). Mutations in all six TFBSs resulted in cell-type-specific changes in expression, but several mutations in the *Gnb3* promoter outside of the known TFBS also resulted in cell-type-specific changes in expression. Thus, other information in the *Gnb3* promoter provides important cell-type context for the functioning of the CRX and E-box motifs.

Our analysis of the *Gnb3* promoter shows that single-binding site and single-nucleotide variants can result in cell-type-specific changes to *cis*-regulation and that scMPRA is a powerful tool for identifying these changes across cell types in mammalian tissues. The *cis*-regulatory logic of the *Gnb3* promoter keeps it expressed at high

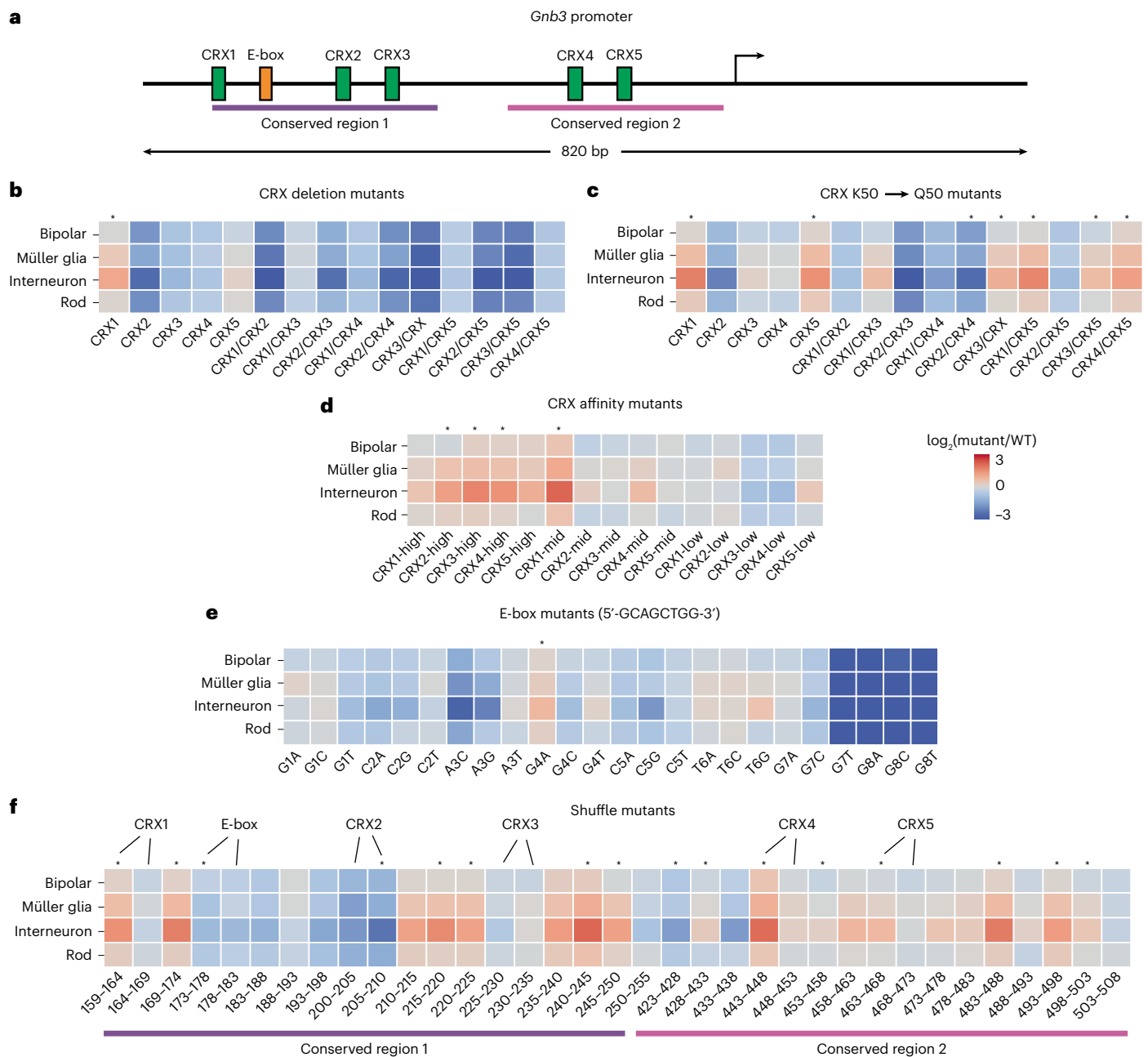


Fig. 6 | Mutations in the *Gnb3* promoter display cell-type-specific effects. a, Schematic of the *Gnb3* promoter showing the location of the five CRX-binding sites and the E-box. **b**, Effects of individual and pairwise deletions of CRX-binding sites. **c**, Effects of individual and pairwise mutations of CRX K50 binding sites to Q50 binding sites. **d**, Effects of changing CRX-binding site affinities. **e**, Effects of saturation mutagenesis of the E-box. **f**, Effects of shuffle mutations in conserved regions of the *Gnb3* promoter. Each region was split into 5 bp windows and the

nucleotides in each window were shuffled. Labels above the heatmap indicate locations where the mutations impact CRX- or E-box binding sites. All plots show \log_2 fold changes of the mutation relative to WT *Gnb3* expression in that cell type. Stars above the plot indicate a significant cell-type-specific effect ($P < 0.01$) calculated by a one-way ANOVA using replicate measurements for each promoter without correction for multiple tests.

levels in rods and bipolar cells in the early postnatal period, and at much lower levels in interneurons, which we speculate is why most cell-type-specific perturbations result in effects of different sizes in interneurons when compared with rods and bipolar cells.

Discussion

We have presented a single-cell MPRA method to measure the cell-type and cell-state-specific effects of CRs. We demonstrated that scMPRA detects cell-type-specific reporter gene activity in a mixed population of cells and in living retinal tissue and cell-state specific activity

in isogenic K562 cells. The assay is reproducible and reports accurate mean levels of reporter gene activity in as few as 75 cells in a complex tissue. New methods that increase the number of single cells measured per experiment³⁸ will increase the size of libraries that can be assayed by scMPRA. The dynamic range was relatively small in this study (eightfold between the strongest and weakest *Gnb3* variants), which may reflect the activity of these specific sequences, but may also arise from the low efficiency of mRNA capture in single cells. scMPRA will therefore benefit from continuing improvements in methods to capture and recover mRNA from single cells.

A key variable in the success of scMPRA experiment will be the efficiency of delivering DNA to the relevant cell types. For tissues with low transfection or transduction efficiencies, most cells will not contain a library member and will therefore be uninformative. This is a problem because of the limited number of cells that can be sequenced with current scRNA-seq protocols. Likewise, if the relevant cell type is rare in the tissue of interest then some enrichment may be necessary to obtain enough cells to make robust measurements. Thus, scMPRA will work best in systems amenable to high-efficiency transfection or transduction. This consideration motivated our choice of the retina as a test system for scMPRA because DNA can be delivered to a large fraction of the cells in an ex vivo retina with high efficiency.

With the burgeoning of Adeno-associated viral delivery systems^{39–43}, we anticipate that the efficiency of DNA delivery will gradually improve for many tissues and systems. Coupling AAV-based methods with scMPRA will allow it to be widely used to study *cis*-regulatory effects in a variety of complex tissues. Given the hypothesis that noncoding variants with cell-type-specific effects underlie a large fraction of human disease, an important application of scMPRA will be to test polymorphisms identified in human genetic studies for cell-type-specific *cis*-regulatory effects.

Online content

Any methods, additional references, Nature Portfolio reporting summaries, source data, extended data, supplementary information, acknowledgements, peer review information; details of author contributions and competing interests; and statements of data and code availability are available at <https://doi.org/10.1038/s41588-022-01278-7>.

References

- Schaub, M. A., Boyle, A. P., Kundaje, A., Batzoglou, S. & Snyder, M. Linking disease associations with regulatory information in the human genome. *Genome Res.* **22**, 1748–1759 (2012).
- Maurano, M. T. et al. Systematic localization of common disease-associated variation in regulatory DNA. *Science* **337**, 1190–1195 (2012).
- Hindorf, L. A. et al. Potential etiologic and functional implications of genome-wide association loci for human diseases and traits. *Proc. Natl Acad. Sci. USA* **106**, 9362–9367 (2009).
- Yang, J. et al. Common SNPs explain a large proportion of the heritability for human height. *Nat. Genet.* **42**, 565–569 (2010).
- Vattikuti, S., Guo, J. & Chow, C. C. Heritability and genetic correlations explained by common SNPs for metabolic syndrome traits. *PLoS Genet.* **8**, e1002637 (2012).
- Shi, H., Kichaev, G. & Pasaniuc, B. Contrasting the genetic architecture of 30 complex traits from summary association data. *Am. J. Hum. Genet.* **99**, 139–153 (2016).
- Aygün, N. et al. Brain-trait-associated variants impact cell-type-specific gene regulation during neurogenesis. *Am. J. Hum. Genet.* **108**, 1647–1668 (2021).
- Nott, A. et al. Brain cell type-specific enhancer–promoter interactome maps and disease-risk association. *Science* **366**, 1134–1139 (2019).
- Spielmann, M. & Mundlos, S. Looking beyond the genes: the role of non-coding variants in human disease. *Hum. Mol. Genet.* **25**, R157–R165 (2016).
- Zhang, F. & Lupski, J. R. Non-coding genetic variants in human disease. *Hum. Mol. Genet.* **24**, R102–R110 (2015).
- Ong, C.-T. & Corces, V. G. Enhancer function: new insights into the regulation of tissue-specific gene expression. *Nat. Rev. Genet.* **12**, 283–293 (2011).
- Arnold, C. D. et al. Genome-wide quantitative enhancer activity maps identified by STARR-seq. *Science* **339**, 1074–1077 (2013).
- Kwasnieski, J. C., Mogno, I., Myers, C. A., Corbo, J. C. & Cohen, B. A. Complex effects of nucleotide variants in a mammalian *cis*-regulatory element. *Proc. Natl Acad. Sci. USA* **109**, 19498–19503 (2012).
- Ireland, W.T. et al. Deciphering the regulatory genome of *Escherichia coli*, one hundred promoters at a time. *eLife* **9**, e55308 (2020).
- Patwardhan, R. P. et al. Massively parallel functional dissection of mammalian enhancers in vivo. *Nat. Biotechnol.* **30**, 265–270 (2012).
- Sharon, E. et al. Inferring gene regulatory logic from high-throughput measurements of thousands of systematically designed promoters. *Nat. Biotechnol.* **30**, 521–530 (2012).
- Kinney, J. B., Murugan, A., Callan, C. G. Jr & Cox, E. C. Using deep sequencing to characterize the biophysical mechanism of a transcriptional regulatory sequence. *Proc. Natl Acad. Sci. USA* **107**, 9158–9163 (2010).
- Melnikov, A. et al. Systematic dissection and optimization of inducible enhancers in human cells using a massively parallel reporter assay. *Nat. Biotechnol.* **30**, 271–277 (2012).
- White, M. A. et al. A simple grammar defines activating and repressing *cis*-regulatory elements in photoreceptors. *Cell Rep.* **17**, 1247–1254 (2016).
- Kwasnieski, J. C., Fiore, C., Chaudhari, H. G. & Cohen, B. A. High-throughput functional testing of ENCODE segmentation predictions. *Genome Res.* **24**, 1595–1602 (2014).
- Chaudhari, H. G. & Cohen, B. A. Local sequence features that influence AP-1 *cis*-regulatory activity. *Genome Res.* **28**, 171–181 (2018).
- Hughes, A. E. O., Myers, C. A. & Corbo, J. C. A massively parallel reporter assay reveals context-dependent activity of homeodomain binding sites in vivo. *Genome Res.* **28**, 1520–1531 (2018).
- Tewhey, R. et al. Direct identification of hundreds of expression-modulating variants using a multiplexed reporter assay. *Cell* **165**, 1519–1529 (2016).
- Hong, C. K. Y. & Cohen, B. A. Genomic environments scale the activities of diverse core promoters. *Genome Res.* **32**, 85–96 (2022).
- Haberle, V. et al. Transcriptional cofactors display specificity for distinct types of core promoters. *Nature* **570**, 122–126 (2019).
- Zabidi, M. A. et al. Enhancer-core-promoter specificity separates developmental and housekeeping gene regulation. *Nature* **518**, 556–559 (2014).
- Love, M. I., Huber, W. & Anders, S. Moderated estimation of fold change and dispersion for RNA-seq data with DESeq2. *Genome Biol.* **15**, 550 (2014).
- Shaffer, S. M. et al. Rare cell variability and drug-induced reprogramming as a mode of cancer drug resistance. *Nature* **546**, 431–435 (2017).
- Moudgil, A. et al. Self-reporting transposons enable simultaneous readout of gene expression and transcription factor binding in single cells. *Cell* **182**, 992–1008 (2020).
- Litzenburger, U. M. et al. Single-cell epigenomic variability reveals functional cancer heterogeneity. *Genome Biol.* **18**, 15 (2017).
- Min, M. & Spencer, S. L. Spontaneously slow-cycling subpopulations of human cells originate from activation of stress-response pathways. *PLoS Biol.* **17**, e3000178 (2019).
- Bonnet, D. & Dick, J. E. Human acute myeloid leukemia is organized as a hierarchy that originates from a primitive hematopoietic cell. *Nat. Med.* **3**, 730–737 (1997).
- Ishikawa, F. et al. Chemotherapy-resistant human AML stem cells home to and engraft within the bone-marrow endosteal region. *Nat. Biotechnol.* **25**, 1315–1321 (2007).
- Friedman, R. Z. et al. Information content differentiates enhancers from silencers in mouse photoreceptors. *eLife* **10**, e67403 (2021).

35. Dixit, A. et al. Perturb-Seq: dissecting molecular circuits with scalable single-cell RNA profiling of pooled genetic screens. *Cell* **167**, 1853–1866 (2016).
36. Murphy, D. P., Hughes, A. E., Lawrence, K. A., Myers, C. A. & Corbo, J. C. Cis-regulatory basis of sister cell type divergence in the vertebrate retina. *eLife* **8**, e48216 (2019).
37. Reese, B. E. Development of the retina and optic pathway. *Vis. Res.* **51**, 613–632 (2011).
38. Cao, J. et al. Comprehensive single-cell transcriptional profiling of a multicellular organism. *Science* **357**, 661–667 (2017).
39. Bryant, D. H. et al. Deep diversification of an AAV capsid protein by machine learning. *Nat. Biotechnol.* **39**, 691–696 (2021).
40. Chan, Y. K. et al. Engineering adeno-associated viral vectors to evade innate immune and inflammatory responses. *Sci. Transl. Med.* **13**, eabd3438 (2021).
41. Byrne, L. C. et al. In vivo-directed evolution of adeno-associated virus in the primate retina. *JCI Insight* **5**, e135112 (2020).
42. Wang, D., Tai, P. W. L. & Gao, G. Adeno-associated virus vector as a platform for gene therapy delivery. *Nat. Rev. Drug Discov.* **18**, 358–378 (2019).
43. Shen, S. Q. et al. Massively parallel cis-regulatory analysis in the mammalian central nervous system. *Genome Res.* **26**, 238–255 (2016).

Publisher's note Springer Nature remains neutral with regard to jurisdictional claims in published maps and institutional affiliations.

Springer Nature or its licensor (e.g. a society or other partner) holds exclusive rights to this article under a publishing agreement with the author(s) or other rightsholder(s); author self-archiving of the accepted manuscript version of this article is solely governed by the terms of such publishing agreement and applicable law.

© The Author(s), under exclusive licence to Springer Nature America, Inc. 2023

Methods

Cell culture

K562 cells were obtained from the Genome Engineering & iPSC Center at Washington University School of Medicine. HEK293 cells (ATCC CRL-1573) were purchased from ATCC (American Type Culture Collection). Cell lines were tested for mycoplasma and were negative. K562 cells were cultured in Iscove's Modified Dulbecco's Medium (Gibco, 12440046) + 10% FBS (Gibco, 10438034) + 1% nonessential amino acids (NEAA; Gibco, 11140050) + 1% penicillin-streptomycin (Gibco, 15140122) at 37 °C with 5% CO₂. HEK293 cells were cultured in Eagle's Minimum Essential Medium (EMEM; ATCC, 30-2003) + 10% FBS (Gibco, 10438034) + 1% penicillin-streptomycin (Gibco, 15140122) at 37 °C with 5% CO₂.

Core promoter library cloning

We developed a two-level barcoding strategy to enable single-cell normalization of plasmid copy number. We applied this strategy to a library of core promoters we previously tested by bulk MPRA²⁴. That core promoter library contains 676 core promoters, each with a length of 133 bp. The library cloning was done in three steps: first, we synthesized a library of 676 core promoters each barcoded with ten different cBCs and cloned this library into a backbone²⁴. In a second step, a dsRed fluorescent reporter cassette was cloned between each core promoter and its associated cBCs as described in ref. 24. Third, we modified this library for scMPRA by adding rBCs downstream of the cBCs, but upstream of the polyA site.

To add the rBCs, we synthesized a single-stranded 90 bp DNA oligonucleotide (oligo) containing a 25 bp random sequence (the rBC), a restriction site and 30 bp homology to the library vector on each side of the rBC region. We used NEBuilder HiFi DNA Assembly Master Mix (E2621) to clone this oligo into the core promoter library. The plasmid library of 4 µg was split into four reactions and digested with 2 µl of Sall for 1.5 h at 37 °C. The digested product was purified with the Monarch Gel Extraction Kit (NEB, T1020). The insert single-stranded DNA was diluted to 1 µM with H₂O. Three assembly reactions were pooled together, each reaction containing 100 ng of digested library backbone, 1 µM of insert DNA, 1 µl of NEBuffer 2, 10 µl of 2X HiFi assembly mix and H₂O up to 20 µl. The reaction was incubated at 50 °C for 1 h. The assembled product was purified with the Monarch PCR & DNA Cleanup kit (NEB, T1030) and eluted in 12 µl of H₂O.

The assembled plasmid was transformed using Gene Pulser Xcell Electroporation Systems by electroporation (Bio-Rad, 1652661) into 50 µl of ElectroMax DH10B electrocompetent cells (Invitrogen, 18290015) with 1 µl of assembled product at 2 kV, 2,000 Ω, 25 nF, with 1 mm gap. SOC medium (Invitrogen, 15544034) of 950 µl was added to the cuvette and then transferred to a 15 ml Falcon tube. Two transformations were performed, and each tube was incubated at 37 °C for 1 h on a rotator with 300 rpm. The culture was then added to prewarmed 150 µl LB/Amp medium and grown overnight at 37 °C. The culture of 1 µl was also diluted 1:100 and 50 µl of the diluted cultured was plated on an LB agar plate to estimate the transformation efficiency. For the core promoter library, we prepared DNA from more than 4 × 10⁸ colonies. Shallow sequencing of this library (below) showed that the majority of library members encoded unique cBC-rBC combinations.

Gnb3 promoter variant library design and cloning

The *Gnb3* library was designed to probe components of the promoter including five binding sites for K50-type homeodomain TFs, an E-box binding site and two evolutionarily conserved regions. We labeled the K50 homeobox sites as Cone Rod Homeobox (CRX) sites because CRX is a K50-homeodomain protein required for *Gnb3* expression and a key-lineage determining factor in retina, even though other K50-type homeobox proteins are also expressed in retinas. To test whether the disruption of CRX sites in the *Gnb3* promoter has cell-type-specific effect, we made the following three types of mutations: (1) all individual and pairwise deletions of the CRX-binding sites by mutating the CRX

sites to 5'-CTACTCCC-3' (ref. 36), (2) all individual and pairwise mutations of CRX-binding sites from K50 homeobox to Q50 homeobox motifs (5'-CTAATTAC-3') and (3) all individual mutations of CRX-binding sites to high (5'-CTAATCCC-3'), medium (5'-CTAAGCCC-3') and low affinity (5'-CTTATCCC-3') K50 homeobox sites²². Our unpublished data suggested that the E-box is important for the *Gnb3* promoter activity and E-box motif is bound by many neuronal-specific TFs³⁷; hence, we mutated each base pair in the E-box to every other base pair and made pairwise mutations of the two core base pairs in the E-box motif. Lastly, we took an unbiased approach to screen for potential cell-type-specific mutations by shuffling mutations across the two conserved regions in the *Gnb3* promoter. Each conserved region was tiled into 5 bp windows, and the nucleotides within each window were shuffled. All library sequences and the corresponding cBCs can be found in Supplementary Table 5.

The library of *Gnb3* promoter variants was constructed in four steps. In the first step, we cloned the *Gnb3* promoter variant library into the core promoter library vector backbone. We ordered double-stranded DNA fragments from Integrated DNA Technologies encoding the varying part of the (520 bp) *Gnb3* promoter and 113 promoter variants. The wild-type *Gnb3* promoter sequence was included twice, each time fused to a different cBC. The DNA fragments were manually pooled and cloned together as a library. In the second step, we cloned the remaining *Gnb3* promoter (300 bp) and mEmerald reporter cassette between the *Gnb3* promoter variants and the first cBC copy using HiFi assembly. In the third step, we used NEB HiFi DNA Assembly Master Mix (NEB, E2621) to insert the U6 promoter between the two copies of the cBCs where it drives expression of the downstream copy of the cBC. In the fourth step, we introduced high-complexity rBCs between the first cBC and the U6 promoter. We synthesized a DNA oligo containing a 25 bp random sequence (rBC), a restriction site and 30 bp homology to the library vector on each side of the rBC barcode region. We then used HiFi Assembly to clone the rBC oligos into the *Gnb3* promoter variant library. In this final library, each plasmid contains a *Gnb3* promoter variant driving mEmerald with a unique cBC-rBC combination in its 3' UTR, which is followed by a polyA signal and the U6 promoter driving a second copy of the cBC, a capture sequence, and a termination signal. A total of eight HiFi Assembly reactions were pooled together to increase the library complexity. This library was transformed and amplified in *Escherichia coli* as described above, and DNA was prepared from 2 × 10⁹ colonies.

Estimating library complexity

To estimate the complexity of the core promoter library, we sequenced the DNA library using a nested PCR-based Illumina library preparation protocol. Briefly, we first used Q5 polymerase (NEB, M0515) to amplify the region containing the two barcodes with SCARED 17 and SCARED P18 (primer sequences can be found in Supplementary Table 7). The total reaction volume was 50 µl using 50 ng of plasmid library with 2.5 µl of 10 µM primer each. After 25 cycles of amplification (61 °C annealing temperature, 30 s extension time), the product was purified with the Monarch PCR & DNA cleanup kit (NEB, T1030) and eluted with 20 µl of ddH₂O. For the second round of PCR, we used the primers SCARED P19 and SCARED P20 in a 25 µl reaction with 0.25 µl product from the previous step (61 °C annealing temperature, 30 s extension time). After ten cycles of amplification, the product was purified using the Monarch PCR & DNA Cleanup kit (NEB, T1030). For the last PCR, we added the P5 and P7 Illumina adapters with SCARED P5, SCARED P7 with ten cycles of amplification in a 25 µl reaction with 2 µl of purified product (65 °C annealing temperature, 30 s extension time). This final product was sequenced on an Illumina MiSeq, and we obtained a total of 1,693,933 reads. After filtering out reads without a cBC or rBC of the correct length, we obtained a total of 1,359,176 reads (80% of the total reads) and 99.5% represented unique cBC-rBC pairs. For the *Gnb3* library, we performed shallow sequencing and obtained a total of 1,939,479 reads.

After filtering out reads without correct cBC or rBC, we obtained a total of 1,838,415 reads (94.7% of the total reads). Among the 1,838,415 correct reads, 99.5% represented unique cBC–rBC pairs.

Estimating the probability of identical cBC–rBC pairs in the same cell

We estimated the probability that more than one copy of a plasmid carrying the same cBC–rBC pair would be transfected into the same cell. We call this probability the collision rate. If the library is transfected into n cells, and a specific cBC–rBC pair is present at m copies in the library, then the expected number of collisions per experiment is given by

$$n^{-m} \sum_{k=0}^n \binom{n}{k} \sum_{q=0}^{n-k} \binom{n-k}{q} \binom{m}{q} q! \left\{ \begin{matrix} m-q \\ n-k-q \end{matrix} \right\}_{n \geq 2} (n-k-q)!(m-q)$$

where k denotes the number of cells that received no plasmid, q denotes the number of cells transfected with exactly one plasmid, parentheses denote the binomial coefficient and brackets denote the partition function. The above expression was simplified by substituting with the bivariate generating function, and the expected number of collisions per experiment is

$$m \left(1 - \left(\frac{n-1}{n} \right)^{m-1} \right)$$

The expected number of collisions per cell (λ) is given by

$$\lambda = \frac{m \left(1 - \left(\frac{n-1}{n} \right)^{m-1} \right)}{n}$$

And, assuming collisions are a Poisson process, the probability of at least one collision in a cell is

$$P(\text{Collision}) = 1 - e^{-\lambda}$$

Using this framework, we can estimate the probability of a collision in our experiment. We assume one million cells (n) are transfected using 10 μg of plasmid DNA and that the effective number of plasmids that enter the nucleus is 10% of that input amount (1 μg)⁴⁴. Plasmid DNA of 1 μg is 2.3×10^{11} . Thus, the value of m in the nucleus is 2.3×10^{11} divided by the number of unique members of the library. This allows us to calculate $P(\text{Collision})$ for a library of any given size. This framework shows that we require a library with 1.6×10^6 unique members to achieve $P(\text{Collision}) = 0.01$. To be 99% sure that a library has at least 1.6×10^6 unique members requires preparing that library 4.5 times as many independent colonies (7.2×10^6), assuming a Poisson distributed library. The core promoter library was prepared from 4×10^8 colonies, 55 times more than required for $P(\text{Collision}) = 0.01$, and the *Gnb3* variant library was prepared from 2×10^9 colonies, 277 times more than required for $P(\text{Collision}) = 0.01$.

Cell line transfections

K562 cells were transfected with the core promoter library using electroporation with the Neon transfection system (Invitrogen, MPK5000). One million cells were transfected with 2 μg of plasmid DNA (mixed-cell experiment) or 10 μg of plasmid DNA (K562 substrate experiment), with three pulses of 1,450 V for 10 ms.

HEK293 cells were transfected with the core promoter library using the Lipofectamine3000 reagent (Invitrogen, L3000001) following the manufacturer's protocol. P3000 reagent of 4 μl , lipofectamine of 4 μl , and OptiMEM were mixed with 2 μg of plasmid DNA to a volume of 250 μl . The lipofectamine reagents and plasmid were mixed and incubated at room temperature for 15 min and then added dropwise to the cells. We collected K562 and HEK293 cells 24 h after transfections for scMPRA.

Ex vivo culturing and transfection of mouse retinas

CD-1IGS mice were obtained from Charles River Laboratory. Following the procedure in ref. 45, retinas from newborn (P0) mice were dissected and electroporated. The sex of the mice could not be determined at the P0 stage. Retinas were dissected in serum-free medium (SFM; 1:1 Dulbecco's Modified Eagle Medium (DMEM):Ham's F12 (Gibco, 11330-032), 100 units per ml penicillin and 100 $\mu\text{g ml}^{-1}$ streptomycin (Gibco, 15140122), 2 mM GlutaMax (Gibco, 35050-061) and 2 $\mu\text{g ml}^{-1}$ insulin (Sigma, I6634) from surrounding sclera and soft tissue leaving the lens in place. Retinas were then transferred to an electroporation chamber (model BTX453 Microslide chamber, BTX Harvard Apparatus modified as described in ref. 46) containing 0.5 $\mu\text{g } \mu\text{l}^{-1}$ of the *Gnb3* promoter variant library 0.5 $\mu\text{g } \mu\text{l}^{-1}$ of a plasmid in which the *Rhodopsin* promoter drives the dsRed fluorophore. For each replicate experiment, three retinas were electroporated. Five square pulses (30 V) of 50-ms duration with 950-ms intervals were applied using a pulse generator (model ECM 830, BTX Harvard Apparatus). Electroporated retinas were removed from the electroporation chamber and allowed to recover in SFM for several minutes before being transferred to the same medium supplemented with 5% fetal calf serum (Gibco, 26140-079). The retinas were then placed (lens side down) on polycarbonate filters (Whatman, 0.2 μm pore size 110,606) and cultured at 37 °C in SFM supplemented with 5% fetal calf serum for 8 d.

Electroporated retinas were collected and dissociated as in ref. 36 with modifications as outlined below. Briefly, three retinas/replicate were washed three times in cold Hanks' Balanced Salt Solution (HBSS) (Gibco, 14025-076) and were then incubated in 400 μl of HBSS containing 0.65 mg papain (Worthington Biochem, LS003126) for 10 min at 37 °C. DMEM of 600 μl (Gibco, 11965-084) containing 10% fetal calf serum (Gibco, 26140-079) was added, and the tissue was gently triturated with P1000 to achieve single cells suspension. One hundred units of DNase1 (Roche, 04716728001) were added to the cell suspension and incubated for an additional 5 min at 37 °C. Cells were centrifuged at 400g for 4 min and then resuspended in 600 ml of sorting buffer (2.5 mM EDTA (Sigma EDS), 25 mM HEPES (Sigma, H3375), 1% BSA (Sigma, H3375) in HBSS) and passed through a 35 μm filter and used directly for fluorescence-activated cell sorting (FACS).

Because the majority of cells in mouse retinas are rod photoreceptors, we attempted to enrich other cell types using FACS. The co-electroporated Rhodopsin-DsRed construct marks rod cells specifically. Therefore, we used FACS to generate a 1:1 mixture of dsRed⁺ to dsRed⁻ cells from dissociated retinas. This procedure should yield a mix of cells in which rod cells comprise 50% of the total cells. In practice, rod cells still comprised 87% of the cells that were analyzed by scMPRA.

Bulk MPRA from cell lines

For both K562 cells and HEK293 cells, we transfected the promoter library as described above, extracted total mRNA and performed reverse transcription using the Superscript IV Reverse Transcriptase Kit (Invitrogen, 18090010). Sequencing libraries were then constructed using the same method of library preparation described above in Estimating Library Complexity from the cDNA and the plasmid library used for transfection. The resulting libraries were sequenced on an Illumina MiSeq instrument. The barcodes were extracted from the reads and tabulated for the RNA and DNA pools. The activity of each library member was computed as $\log_2(\text{RNA counts}/\text{DNA counts})$. The activities of barcodes linked to the same core promoter were averaged to calculate the final activity of each promoter.

scRNA-seq for scMPRA

To perform scMPRA, we targeted 2,000 cells from the HEK/K562 mixed pool per replicate for each mixed-cell experiment, 2,500 cells per replicate for the K562-only experiment, and 2,500 cells (after sorting) per replicate for the retina experiment. The cells were prepared according to the manufacturer's instructions for the 10x Chromium Single Cell 3'

Feature Barcode Library Kit (PN-1000079), with the changes we made detailed below.

Our goal was to both quantify the cBC–rBC pairs from each single cell and sequence the cellular mRNAs from those same single cells. We captured all polyadenylated RNAs (barcoded reporter RNAs and cellular mRNAs) from single cells following the manufacturer’s protocol up to the cDNA amplification step.

For the cellular mRNAs (transcriptome), we followed the 10x protocol, using 1/4 of the cDNA library to generate dual-indexed transcriptomes. To quantify the cBC–rBC pairs, we performed separate PCRs using primers specifically targeting the reporter gene to improve barcode recovery efficiencies. Because the 10x protocol only uses 1/4 of the generated cDNA, we separately amplified the barcodes from another 1/4 of the pellet cleanup. We first used Q5 polymerase (NEB, M0515) to amplify the region containing the cBC–rBC pairs with SCARED P17 and SCARED P18 with ten cycles (61 °C annealing temperature, 30 s extension time). The sample was divided equally into eight PCR reactions, each with 50 µl of total volume to reduce possible jackpotting. The product was then purified with the Monarch PCR & DNA Cleanup kit (NEB, T1030) and eluted with 20 µl of ddH₂O. We then added sequencing adapters using an additional two rounds of PCR. The first adapter PCR was performed with SCARED P21 and SCARED PP2 with a total of 10 ng of product from the barcode PCR (61 °C annealing temperature, 30 s extension time). Again, we pooled eight PCR reactions, each with 50 µl of total volume and ten PCR cycles. The PCR product was purified using the Monarch PCR & DNA Cleanup kit (NEB, T1030). For the last PCR, to add the P5 and P7 Illumina adapters, we used the primers SCARED P45, SCARED PP3 with 10 ng of product and pooled eight PCR reactions, each with 50 µl of total volume and ten PCR cycles (58 °C annealing temperature, 30 s extension time).

For the U6 promoter library construction, we followed step 4 of the 10x feature barcoding library preparation protocol (Chromium Next GEM Single Cell 3’ Reagent Kits v3.1 (Dual Index) CG000316 Rev C) as written.

The transcriptome and barcode libraries were mixed in equimolar ratios and paired-end sequencing was performed on the Illumina Next-Seq 500 with 28 × 105 paired-end reads. Read1 was limited to 28 bp to avoid sequencing the constant poly(A) sequence.

scRNA-seq data processing

The scRNA-seq data were processed using Cellranger 6.0.1 (<https://github.com/10xGenomics/cellranger>) and Scanpy 1.8.1 (ref. 47) (<https://github.com/theislab/scanpy>) following the standard pipeline. Briefly, different sequencing runs from the same biological replicate were pooled together and processed with CellRanger 6.1.1; the final output expression matrix was then imported into Scanpy for further processing. We first removed cells with less than 1,000 genes, genes that were present in less than three cells, and cells with high counts of mitochondrial genes. Next, we normalized the UMI counts to the total cell UMI counts. The normalized expression matrix was used for clustering and visualization with Scanpy.

scMPRA data processing

For each promoter library, paired-end reads generated from barcoded reporter RNAs were processed with custom scripts that can be found on GitHub (<https://github.com/barakcohenlab/scMPRA>). In each paired-end read, Read1 contains a 10x cell barcode and a UMI, while Read2 contains the cBC and rBC sequences. We define a ‘quad’ as a 10x cell barcode, UMI, cBC and rBC originating from the same individual paired-end read. To tabulate the cBC–rBCs, we first matched the constant sequences flanking both barcodes, filtering out reads where either barcode was not the correct length. We performed this filtering using a stand-alone program (https://github.com/szhao045/scMPRA_parsingtools). Second, we filtered out incorrect 10x cell barcodes based on the CellRanger output barcode list using error correction with a maximum Hamming distance

of one. Third, to mitigate the effect of template switching during the PCR steps, we plotted the rank read depth for each unique quad and identified an ‘elbow point’ at a minimum depth of one read for the mixed-cell and the retina experiment and ten reads for the K562 alone experiment. We kept all reads above the minimum depth and kept a low-depth unique quad if it contained a cBC–rBC matching a high-depth pair with a Hamming distance of at most one. Lastly, for the mixed-cell experiment and the K562 cell alone experiment, we removed any cell with less than 100 scMPRA-associated UMIs because the scMPRA reads from those cells were poorly sampled. For the last step, because the retina experiment contains additional information from the U6 promoter, we did not threshold based on the cells. Because U6 promoter data provide information on whether a given cBC in a given cell is sampled well, we removed all unique barcode pairs containing only one UMI for a cBC.

Calculating the single-cell activities of promoters

Once the high-confidence quads were identified, we computed A , the activity of a promoter in an individual cell using

$$A = \frac{\sum_{i=1}^n \text{UMI count for cBC}_i}{\sum_{i=1}^n \text{rBC count for cBC}_i}$$

where n is the number of unique cBCs that mark a single promoter in the library, and the UMI and rBC counts are summed over all quads with a given 10x cell barcode. We then compute C , the cell-type-specific activity of a promoter as

$$C = \frac{\sum_{j=1}^m A_j}{m}$$

where m is the number of cells in a given cell type, and all 10x cell barcodes assigned to a given cell type are identified from their matched scRNA-seq profiles. For scMPRA data from the retina, we modified the equation for cell-type-specific activity as follows

$$C = \frac{\sum_{j=1}^P A_j}{P + U}$$

where P is the number of cells of a given cell type in which *Gnb3*-driven cBCs were detected and U is the number of cells of that cell type for which a U6 promoter cBC was detected without detecting any corresponding *Gnb3*-driven cBC. This modification has the effect of adding activities of zero for all cells with U6-driven cBCs that did not express a *Gnb3*-driven cBC.

Cell cycle analysis

Cell cycle analysis for the scRNA-seq experiment was done with Scanpy 1.8.1 with cell cycle genes⁴⁸. The expression profile of each cell was projected onto a PCA plot based on the list of cell cycle genes using Scanpy.

Motif analysis

The core promoters were first clustered according to their expression levels in the different cell substate populations by hierarchical clustering. We categorized our data into upregulated/downregulated clusters at the first branching point, aiming to preserve the large structure. We then identified core promoter motifs in each promoter using the parameters for each motifs position weight matrix as described in ref. 26 with MAST v4.10.0 (ref. 49) and plotted the proportion of promoters containing each motif in each promoter class.

Statistical analyses

All statistical analyses were done using Python 3.9.6, Numpy 1.12.1 (ref. 50), Scipy 1.6.3 and R 4.0.2. For all boxplots presented in this manuscript, the bounds of the box represent the upper and lower quartiles, and the center line represents the median. The whiskers extend to the

maxima/minima except for points determined to be outliers using a method that is a function of the interquartile range⁵¹.

Ethics

This study was performed in strict accordance with the recommendations in the Guide for the Care and Use of Laboratory Animals of the National Institutes of Health. All of the animals were handled according to protocol A-3381-01 approved by the Institutional Animal Care and Use Committee of Washington University in St. Louis. Euthanasia of mice was performed according to the recommendations of the American Veterinary Medical Association Guidelines on Euthanasia. Appropriate measures were taken to minimize pain and discomfort to the animals during experimental procedures.

Reporting summary

Further information on research design is available in the Nature Portfolio Reporting Summary linked to this article.

Data availability

Next-generation sequencing data that support the findings of the study are available in the Gene Expression Omnibus using accession code [GSE188639](https://www.ncbi.nlm.nih.gov/geo/query/acc.cgi?acc=GSE188639).

Code availability

The code that supports the findings of this study is available in Zenodo⁵².

References

- Cohen, R. N., van der Aa, M. A. E. M., Macaraeg, N., Lee, A. P. & Szoka, F. C. Jr. Quantification of plasmid DNA copies in the nucleus after lipoplex and polyplex transfection. *J. Control. Release* **135**, 166–174 (2009).
- Hsiao, T. H.-C. et al. The *cis*-regulatory logic of the mammalian photoreceptor transcriptional network. *PLoS One* **2**, e643 (2007).
- Montana, C. L., Myers, C. A. & Corbo, J. C. Quantifying the activity of *cis*-regulatory elements in the mouse retina by explant electroporation. *J. Vis. Exp.*(52), 2821 (2011).
- Wolf, F. A., Angerer, P. & Theis, F. J. SCANPY: large-scale single-cell gene expression data analysis. *Genome Biol.* **19**, 15 (2018).
- Tirosh, I. et al. Dissecting the multicellular ecosystem of metastatic melanoma by single-cell RNA-seq. *Science* **352**, 189–196 (2016).
- Bailey, T. L. & Gribskov, M. Combining evidence using *P* values: application to sequence homology searches. *Bioinformatics* **14**, 48–54 (1998).
- Harris, C. R. et al. Array programming with NumPy. *Nature* **585**, 357–362 (2020).
- Waskom, M. Seaborn: statistical data visualization. *J. Open Source Softw.* **6**, 3021 (2021).

- Zhao, S. et al. A single-cell massively parallel reporter assay detects cell type specific *cis*-regulatory activity. <https://doi.org/10.5281/zenodo.7338678> (2022).

Acknowledgements

We thank the members of the Cohen laboratory for their critical feedback on the manuscript. We thank J. Hoisington-Lopez and M. Crosby for assistance with high-throughput sequencing. This work is supported by grants to B.A.C. from the National Institutes of Health (R01 GM140711 and R01 GM092910) and to J.C.C. from the National Institutes of Health (R01 EY030075). The funders had no role in study design, data collection and analysis, decision to publish or preparation of the manuscript.

Author contributions

S.Z. and B.A.C. conceived and designed the project. All experiments and analyses were performed by S.Z. with technical contributions from C.K.Y. H. and D.M.G., except for the electroporation and culturing of mouse retinas, which was performed by C.A.M. J.C.C. and M.A.W. provided critical input into the design of the *Gnb3* promoter variant library. S.Z., C.K.Y.H. and B.A.C. wrote the manuscript with input and feedback from all authors.

Competing interests

S.Z. and B.A.C. are inventors on a pending patent filed by Washington University in St. Louis which may encompass the methods, reagents and data disclosed in this manuscript. B.A.C. is on the scientific advisory board of Patch Biosciences. The remaining authors declare no competing interests.

Additional information

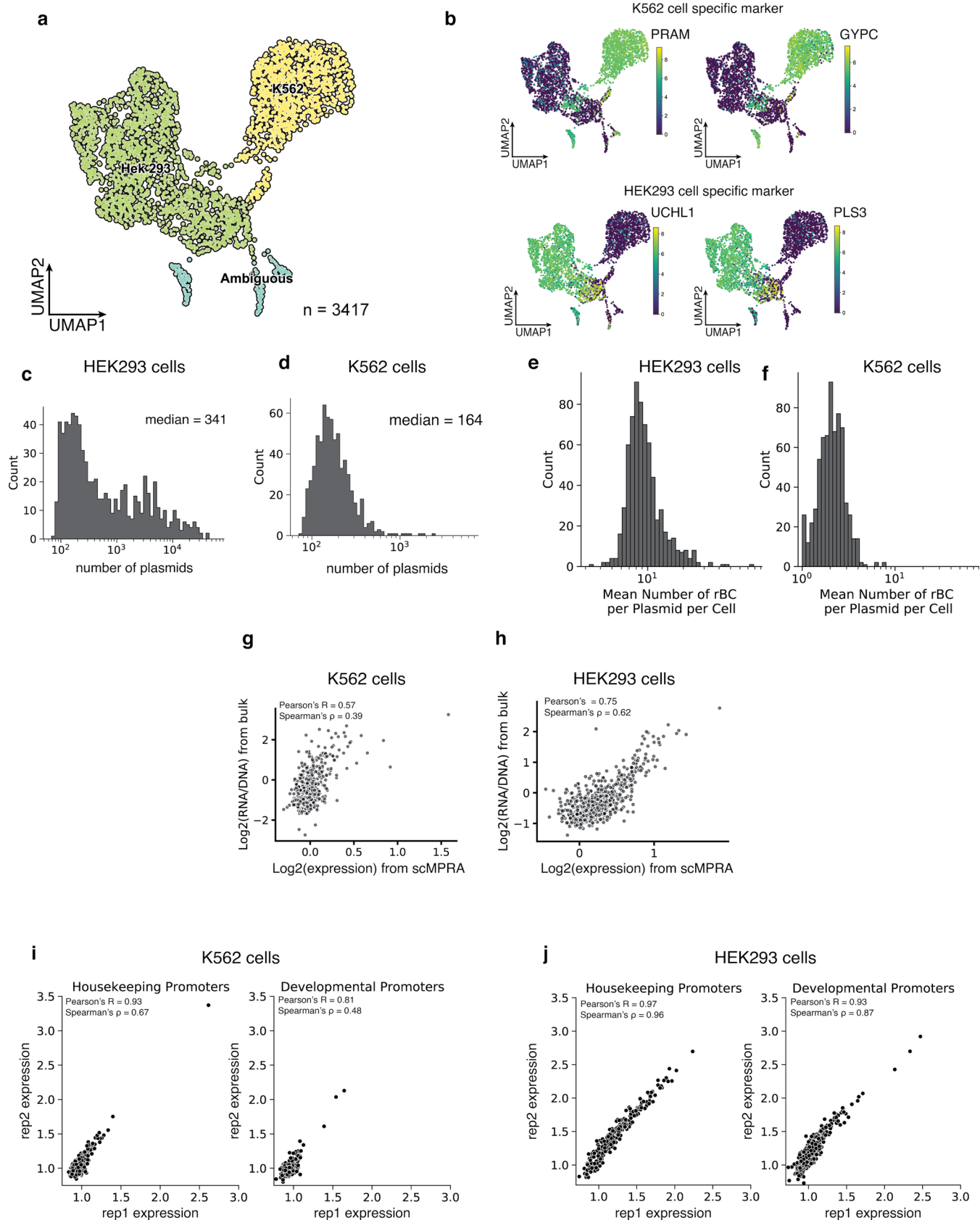
Extended data is available for this paper at <https://doi.org/10.1038/s41588-022-01278-7>.

Supplementary information The online version contains supplementary material available at <https://doi.org/10.1038/s41588-022-01278-7>.

Correspondence and requests for materials should be addressed to Barak A. Cohen.

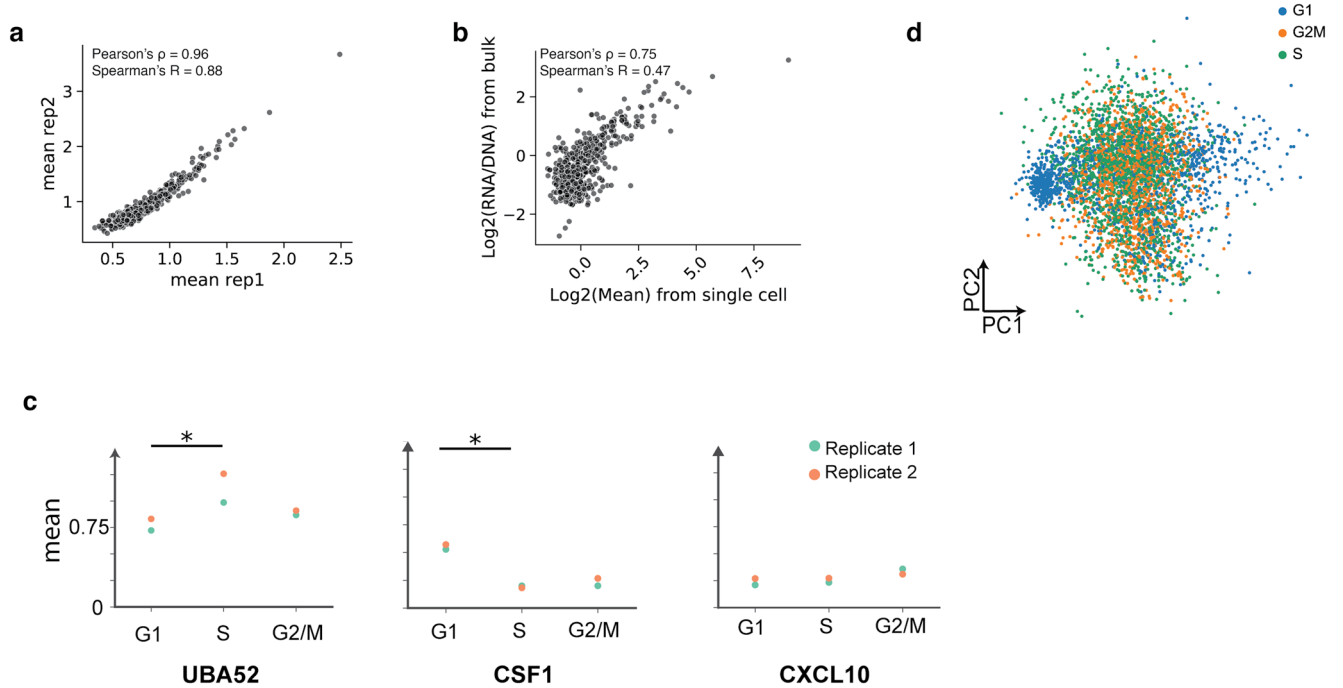
Peer review information *Nature Genetics* thanks Bas van Steensel, Rickard Sandberg and the other, anonymous, reviewer(s) for their contribution to the peer review of this work.

Reprints and permissions information is available at www.nature.com/reprints.



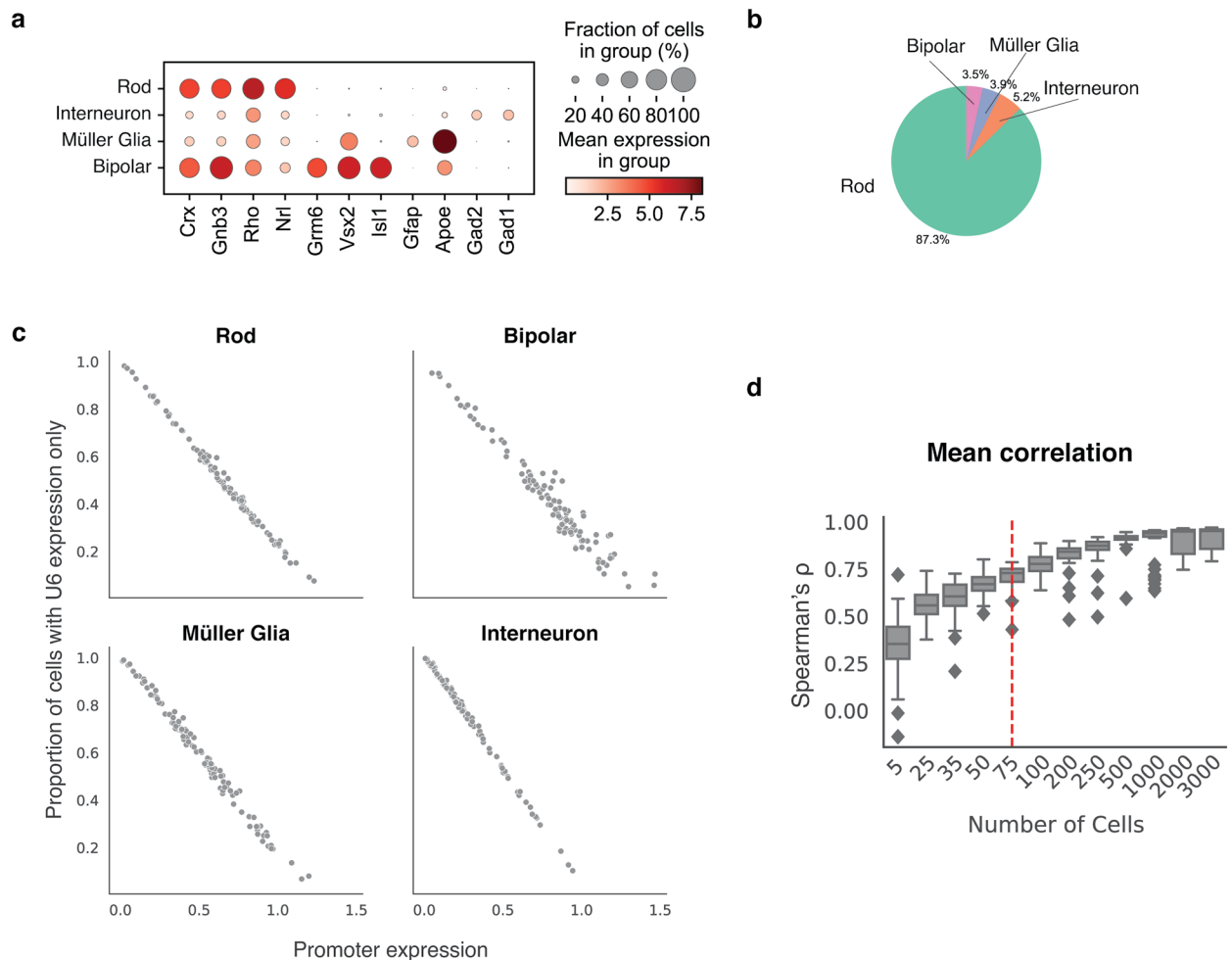
Extended Data Fig. 1 | scMPRA measures cell-type specific CRS activity. (a) UMAP of the single-cell transcriptome from the mixed-cell experiment. 105 out of 3417 cells (3%) are labeled by both K562 and HEK293 cell genes. (b) UMAP of the mixed-cell experiment with cells marked by other representative markers for K562 and HEK293 cell expression. (c, d) Histogram of the number of plasmids (unique cBC-rBC pairs) transfected into K562 cells and HEK293

cells. (e, f) Histogram of the mean number of rBC per cBC (CRS) per cell for K562 cells and HEK293 cells. (g, h) Correlation of bulk MPRA versus scMPRA where only the scMPRA data has been UMI normalized. (i, j) Scatterplot of scMPRA reproducibility for housekeeping and developmental promoters in K562 cells and HEK293 cells.



Extended Data Fig. 2 | scMPRA measures CRS activity in K562 cell substates. (a) Reproducibility for mean expression of core promoters in K562 cells. (b) Correlation of bulk and scMPRA (non-UMI corrected) in K562 cells (c) Different dynamics of expression. For UBA52, the promoter is most highly expressed in S phase, whereas for CSF1, the promoter is most highly expressed in G1 phase.

For CXCL10, the promoter is expressed evenly through cell cycle (Stars indicate significance from two-sided Wilcoxon rank sum test, *: $p < 0.05$) (d) Cells no longer cluster together based on cell cycle genes after the effects of the cell cycle are removed.



Extended Data Fig. 3 | Robust measurements of *Gnb3* promoter library in ex vivo retina. (a) Expression of marker genes by scRNA-seq used to identify cell types in the retina. (b) Percentage of the total cells recovered represented by each retinal cell type. (c) Plot showing the relationship between the mean activity of a *Gnb3* promoter variant in a given cell type (x-axis) and the proportion of cells in which that promoter variant is silent (y-axis). Individual cells in which a given *Gnb3* variant is silent are identified as cells with U6-expressed cBC, but no

Gnb3-expressed cBC. (d) The correlation between biological replicates ($n = 2$) is plotted as a function of the number of cells used in the analysis. The bounds of the box represent the upper and lower quartiles respectively, and the center line represents the median. The whiskers extend to the maxima/minima except for points determined to be outliers using a method that is a function of the interquartile range.

Reporting Summary

Nature Portfolio wishes to improve the reproducibility of the work that we publish. This form provides structure for consistency and transparency in reporting. For further information on Nature Portfolio policies, see our [Editorial Policies](#) and the [Editorial Policy Checklist](#).

Statistics

For all statistical analyses, confirm that the following items are present in the figure legend, table legend, main text, or Methods section.

n/a Confirmed

- The exact sample size (n) for each experimental group/condition, given as a discrete number and unit of measurement
- A statement on whether measurements were taken from distinct samples or whether the same sample was measured repeatedly
- The statistical test(s) used AND whether they are one- or two-sided
Only common tests should be described solely by name; describe more complex techniques in the Methods section.
- A description of all covariates tested
- A description of any assumptions or corrections, such as tests of normality and adjustment for multiple comparisons
- A full description of the statistical parameters including central tendency (e.g. means) or other basic estimates (e.g. regression coefficient) AND variation (e.g. standard deviation) or associated estimates of uncertainty (e.g. confidence intervals)
- For null hypothesis testing, the test statistic (e.g. F , t , r) with confidence intervals, effect sizes, degrees of freedom and P value noted
Give P values as exact values whenever suitable.
- For Bayesian analysis, information on the choice of priors and Markov chain Monte Carlo settings
- For hierarchical and complex designs, identification of the appropriate level for tests and full reporting of outcomes
- Estimates of effect sizes (e.g. Cohen's d , Pearson's r), indicating how they were calculated

Our web collection on [statistics for biologists](#) contains articles on many of the points above.

Software and code

Policy information about [availability of computer code](#)

Data collection

Data analysis

For manuscripts utilizing custom algorithms or software that are central to the research but not yet described in published literature, software must be made available to editors and reviewers. We strongly encourage code deposition in a community repository (e.g. GitHub). See the Nature Portfolio [guidelines for submitting code & software](#) for further information.

Data

Policy information about [availability of data](#)

All manuscripts must include a [data availability statement](#). This statement should provide the following information, where applicable:

- Accession codes, unique identifiers, or web links for publicly available datasets
- A description of any restrictions on data availability
- For clinical datasets or third party data, please ensure that the statement adheres to our [policy](#)

Human research participants

Policy information about [studies involving human research participants and Sex and Gender in Research](#).

Reporting on sex and gender

Use the terms *sex* (biological attribute) and *gender* (shaped by social and cultural circumstances) carefully in order to avoid confusing both terms. Indicate if findings apply to only one sex or gender; describe whether sex and gender were considered in study design whether sex and/or gender was determined based on self-reporting or assigned and methods used. Provide in the source data disaggregated sex and gender data where this information has been collected, and consent has been obtained for sharing of individual-level data; provide overall numbers in this Reporting Summary. Please state if this information has not been collected. Report sex- and gender-based analyses where performed, justify reasons for lack of sex- and gender-based analysis.

Population characteristics

Describe the covariate-relevant population characteristics of the human research participants (e.g. age, genotypic information, past and current diagnosis and treatment categories). If you filled out the behavioural & social sciences study design questions and have nothing to add here, write "See above."

Recruitment

Describe how participants were recruited. Outline any potential self-selection bias or other biases that may be present and how these are likely to impact results.

Ethics oversight

Identify the organization(s) that approved the study protocol.

Note that full information on the approval of the study protocol must also be provided in the manuscript.

Field-specific reporting

Please select the one below that is the best fit for your research. If you are not sure, read the appropriate sections before making your selection.

Life sciences Behavioural & social sciences Ecological, evolutionary & environmental sciences

For a reference copy of the document with all sections, see nature.com/documents/nr-reporting-summary-flat.pdf

Life sciences study design

All studies must disclose on these points even when the disclosure is negative.

Sample size

For the cell culture experiments we included two biological replicates in order to compute a correlation. A total of 676 cis-regulatory sequences were tested, with each sequence being represented by 10 DNA barcodes.

For the retina experiments we included two biological replicates in order to compute a correlation. Each replicate contained three retinas. A total of 115 cis-regulatory sequences were tested, with each sequence being represented by 1 DNA barcode.

Data exclusions

Sequencing reads from 10X single-cell transcriptome data were filtered based on standard 10X cell ranger pipeline. Cells with less than 100 genes and genes with less than 3 cells were removed. Cells presenting transcription signature of both cell types were removed as they were likely duplets. Sequencing reads from cis-regulatory sequence (CRS) library were filtered based on (i) whether they are present in the cells with well-measured transcriptome, (ii) whether they have enough depth (minimum: 1 for mixed cell experiment and 10 for k562 alone experiment), (iii) whether each CRS is measured in more than 100 cells. Those criteria are commonly used for single-cell RNA-seq data processing and Massively Parallel Reporter Assay data processing.

Replication

Two replicates were included in the study and both were successful.

Randomization

Randomization was not applicable because the same library was used in each experiment.

Blinding

Blinding was not applicable because the same library was used in each experiment.

Reporting for specific materials, systems and methods

We require information from authors about some types of materials, experimental systems and methods used in many studies. Here, indicate whether each material, system or method listed is relevant to your study. If you are not sure if a list item applies to your research, read the appropriate section before selecting a response.

Materials & experimental systems

Methods

- n/a Involved in the study
- Antibodies
- Eukaryotic cell lines
- Palaeontology and archaeology
- Animals and other organisms
- Clinical data
- Dual use research of concern

- n/a Involved in the study
- ChIP-seq
- Flow cytometry
- MRI-based neuroimaging

Eukaryotic cell lines

Policy information about [cell lines and Sex and Gender in Research](#)

Cell line source(s)	Human K562 cell line was obtained from the Genome Engineering & iPSC Center at Washington University School of Medicine; Human HEK293 cell line was obtained from ATCC (catalog number CRL-1573).
Authentication	Neither cell line was authenticated
Mycoplasma contamination	Both cell lines tested negative for Mycoplasma
Commonly misidentified lines (See ICLAC register)	no commonly misidentified cell lines were used

Animals and other research organisms

Policy information about [studies involving animals](#); [ARRIVE guidelines](#) recommended for reporting animal research, and [Sex and Gender in Research](#)

Laboratory animals	CD-1 mice from Charles River Laboratory were used in this study. Retinas from P0 mice were used. The sex of the mice were not determined because it is difficult to determine the sex of P0 mice.
Wild animals	No wild animals were used in this study.
Reporting on sex	Because it is difficult to determine the sex of P0 mice the mice were not sexed before harvesting the retinas
Field-collected samples	No field-collected samples were used in this study
Ethics oversight	This study was performed in strict accordance with the recommendations in the Guide for the Care and Use of Laboratory Animals of the National Institutes of Health. All of the animals were handled according to protocol# A-3381-01 approved by the Institutional Animal Care and Use Committee of Washington University in St. Louis. Euthanasia of mice was performed according to the recommendations of the American Veterinary Medical Association Guidelines on Euthanasia. Appropriate measures are taken to minimize pain and discomfort to the animals during experimental procedures.

Note that full information on the approval of the study protocol must also be provided in the manuscript.

Flow Cytometry

Plots

Confirm that:

- The axis labels state the marker and fluorochrome used (e.g. CD4-FITC).
- The axis scales are clearly visible. Include numbers along axes only for bottom left plot of group (a 'group' is an analysis of identical markers).
- All plots are contour plots with outliers or pseudocolor plots.
- A numerical value for number of cells or percentage (with statistics) is provided.

Methodology

Sample preparation	Mice retinas were dissociated and sorted for GFP+/DsRed+ and GFP+/DsRed- populations in a 1:1 ratio
Instrument	Cytoflex SRT
Software	NA
Cell population abundance	NA

Gating strategy

Supplementary Figure 1 now shows the gating strategy

Tick this box to confirm that a figure exemplifying the gating strategy is provided in the Supplementary Information.